Origin of Au $L\beta_2$ visible satellites

H. Oohashi,* T. Tochio, and Y. Ito
Laboratory of Atomic & Molecular Physics, Institute for Chemical Research, Kyoto University, Gokasho Uji 611-0011, Japan

A. M. Vlaicu
National Institute for Material Science, SPring-8, Mikazuki, Hyogo 679-5198, Japan

(Received 17 July 2002; revised manuscript received 3 June 2003; published 10 September 2003)

Measurements of $L\beta$ spectra of gold using a high-resolution single-crystal x-ray spectrometer are presented. Energy values and intensities of the $L\beta_2$ satellite lines are confirmed by fitting Voigt functions to the observed spectra. Relative intensity ratios of $L\beta_2$, $L\beta_3$, $L\beta_{15}$, and $L\beta_2$ satellite lines are investigated at various excitation energies. The origin of the $L\beta_2$ satellite lines, $L\beta_2'$ and $L\beta_2''$, are confirmed to be mainly due to the L-LM Coster-Kronig transition, with intensities closely related to the photoionization cross section of the subshell L_1.

DOI: 10.1103/PhysRevA.68.032506 PACS number(s): 32.30.Rj, 32.80.Hd

I. INTRODUCTION

X-ray emission spectroscopy is very useful for investigating atomic electron states. In particular, fine structure of emission spectra, such as satellite lines, reflect various physical phenomena. One of the origins of satellite lines is generally believed to be radiative transitions due to multiple vacancies. Two processes can be thought of as the causes of multiple vacancies. One is the shake process, which is the ionization (shake-off) or excitation (shake-up) of outer-shell electrons during ionization of inner-shell electrons by photons or charged particles. The shake process can occur during excitation, with a probability that depends on excitation energy, when it is not far above the threshold (the probability becomes independent of excitation energy when it is high enough). A number of models have been proposed for the energy dependence of shake-off probability, such as the Thomas model [1]. The second process that can cause multiple vacancies is nonradiative transitions, such as Coster-Kronig transitions. This is a relaxation process that is independent of excitation energy. Therefore, measurement of the excitation energy dependence of satellite lines is significant in the investigation of the origins of these lines. Measurement of L x-ray emission spectra related to Coster-Kronig transitions plays an important role in such work.

X-ray emission spectra of heavy elements have been less extensively studied than those of low-Z elements. Although gold is very important in various applications, studies of Au L x-ray spectra are rather scarce [2–6]. To the best of our knowledge, only a single paper has been published on the satellite lines of Au [5].

The L-LM Coster-Kronig transitions are forbidden in elements having a certain range of Z numbers. According to the calculations of Chen [7], L-LM Coster-Kronig transitions in elements with $50 \leqslant Z \leqslant 74$ are forbidden energetically. However, a ${}_{74}$W $L\beta_2$ satellite line has been reported [8–10], with this visible satellite confirmed to be mainly due to the L-LM Coster-Kronig transition.

In the present study, the structure of ${}_{79}$Au $L\beta_2$ spectrum is reported. Energies and intensities of Au $L\beta_2$ diagram lines were obtained by electron bombardment using a single-crystal high-resolution x-ray spectrometer for comparison with theoretical calculations. In addition, measurements were conducted using various incident electron energies for satellites in the higher-energy region of $L\beta_2$ to elucidate the origins of these satellites.

Initial and final vacancies of the measured diagram and satellite lines are shown in Table I.

II. EXPERIMENT

A. Experimental setup

Gold L spectral lines were excited by electron bombardment using a rotating anode. Spectra were measured at excitation voltages of 25∼55 kV and tube currents of 50 or 100 mA. Excitation energies gained at those voltages can ionize electrons from the Au L_1 shell, which has a binding energy of 14 352.8 eV [11]. Spectral measurements were conducted using a single-crystal spectrometer containing a symmetric Si(440) perfect crystal. A double slit collimator of length 100 mm and vertical width 20 μm was used for measurements. Measuring period was selected to give approximately 10 000 counts at the peak position of the $L\beta_2$ diagram line. Values by Bearden [12] were used as a reference for the diagram

TABLE I. Initial and final states of each transition of the measured lines.

Emission line	Initial vacancy	Final vacancy
$L\alpha_1$	L_3	M_5
$L\alpha_2$	L_3	M_4
$L\beta_1$	L_2	M_4
$L\beta_2$	L_3	N_5
$L\beta_3$	L_1	M_3
$L\beta_{15}$	L_3	N_4
$L\beta_2'$	L_3M_5	M_5N_5
$L\beta_2''$	L_3M_4	M_4N_5

*Electronic address: hirof@elec.kuicr.kyoto-u.ac.jp

line. Spectral lines were measured using an $Ar_{0.9}(CH_4)_{0.1}$ flow proportional counter (FPC).

To estimate the contribution of line broadening by the spectrometer, the same lines need to be measured using another system. A double-crystal spectrometer system was used to measure $L\alpha_{1,2}$ diagram lines. The double-crystal spectrometer has excellent resolving power [13], and is therefore suitable for comparing the diagram lines measured by the single-crystal spectrometer. Fluorescence x-ray spectra of $L\alpha_{1,2}$ in Au were measured using a double-crystal spectrometer (Rigaku System 3580 E3). Si(220) reflections were used in both crystals. The sample was 50-μm-thick metallic foil. Primary x-ray tube load was 40 kV and 70 mA. Spectra were also measured using FPC.

B. Data analysis

No smoothing was applied to the raw data. Two satellite lines caused by a spectator hole in the M_4 or M_5 subshell were different enough in energy to be measured separately from the $L\beta_2$ line and could be fitted independent of the $L\beta_2$ line. These are called "visible satellites." However, satellite lines that arise from the presence of a spectator hole in the N shell or outer shell are very close to the $L\beta_2$ line. These are called "hidden satellites." As in the case of gold, the $L\beta_3$ line appeared at a slightly higher energy than that of the $L\beta_2$ line, making separation of the hidden satellites from the $L\beta_2$ line very difficult.

Therefore, energy shifts and relative intensities of hidden satellites in the fitting analyses were fixed. Measured spectra of the $L\beta_{2,15,3}$, L_3M_5-M_5N_5 satellite, and L_3M_4-M_4N_5 satellite were analyzed using five Voigt functions. Because the $L\beta_2$ line includes hidden satellites, Voigt functions were used for $L\beta_2$ to describe the multiplet of the diagram line and seven hidden satellites (see Sec. III A, Refs. [9,14]), namely, L_3N_i-$N_iN_5(i=1-7)$. Other satellites caused by a spectator hole in the O shell or P shell were not included in the multiplet, because they have almost the same energy as the diagram line. All satellites were assumed to have the same width as that of the diagram line. Spectra obtained at 25 kV and 45 kV are shown in Fig. 1 together with analysis results.

III. RESULTS AND DISCUSSION

A. Diagram lines

In Table II, the measured values of the width at half maximum (FWHM) of the Au L emission lines are compared to other experiments and theory [2,3,6,15]. The natural width of an x-ray line originating from a transition from atomic level (A) to level (B) is given by the sum of the widths of the initial and final levels:

$$\Gamma(A-B)=\Gamma(A)+\Gamma(B). \tag{1}$$

The values recommended by Campbell and Papp [15] are used as the natural linewidths of atomic vacancy states.

Experimental values of natural linewidths of diagram lines were obtained using the multiplet fitting method of Deutsch *et al.* [14] and Vlaicu *et al.* [9]. Both Lorentzian and Voigt functions were used in the spectral analysis:

$$I(E)=\sum_{m=1}^{M} A_m \sum_{l=1}^{L} p_l(E,E_{lm}-s_m,b_{lm},w_m,d_m), \tag{2}$$

where $p(E)$ can be a Lorentzian or Voigt profile.

In Eq. (2), the indices m denote multiplets and the indices l represent lines within given multiplets. Prior to fitting, the positions of diagram and satellite lines E_{lm} and the intensities b_{lm} of the satellite lines relative to the diagram lines need to be calculated, as these are all fixed parameters in the fitting procedure. Within a multiplet, the amplitude A_m, energy shift s_m relative to the calculated position, width w_m, and dispersion d_m are common to all lines. Amplitude, energy shift, and width parameters are unconstrained during the fitting. Dispersion parameters were set to the values calculated for each diagram line from the geometry of the collimator and the dispersion of the crystal.

Equations of the relative intensities of the satellites are given in Sec. III B. Since $L\alpha_1$ and $L\alpha_2$ spectra are transitions from L_3 vacancy states, the multiple vacancy states before radiative transition can be the same as those of $L\beta_2$. Thus, these are thought to involve the same number of hidden satellites as $L\beta_2$. The relative intensities of satellite lines contributing to the two lines are assumed to be the same as for $L\beta_2$. Multiplet fitting was performed on the three lines.

From observations of $L\alpha$ width using both single- and double-crystal spectrometers, instrumental functions of each spectrometer were obtained. Assuming that these were the actual dispersion parameters due to the collimator and crystal, dispersion parameters were recalculated for each $L\beta$ diagram line. Natural widths obtained in this way are shown in parentheses in Table II.

Theoretical values shown in Table II are the sums of level widths before and after transition [see Eq. (1)]. Because the diagram lines actually include hidden satellite lines, the measured diagram lines have different FWHM to the theoretical values. In contrast, FWHM that were measured using the double-crystal spectrometer are considered to be slightly influenced by the instrumental function. This effect can be ignored, especially for lines with large FWHM, such as the L lines of heavy elements [13].

The FWHM of $L\alpha_{1,2}$ measured using single- and double-crystal spectrometers are in good agreement, with differences less than 5%. Note that fitting to Voigt profiles was able to correctly compensate for line broadening by the spectrometer.

B. Satellites

Energy positions of the satellite lines of high-Z elements are given in a table published by Parente *et al.* [16]. However, values for gold are not given in this table. Values for the energy shifts of satellite lines in gold were thus obtained by taking averages of the values for platinum and mercury.

Relative intensities of the satellite lines were calculated assuming that the fluorescence yields $\omega_{i,i=1,2,3}$ are the same for both single vacancy states and multiple vacancy states

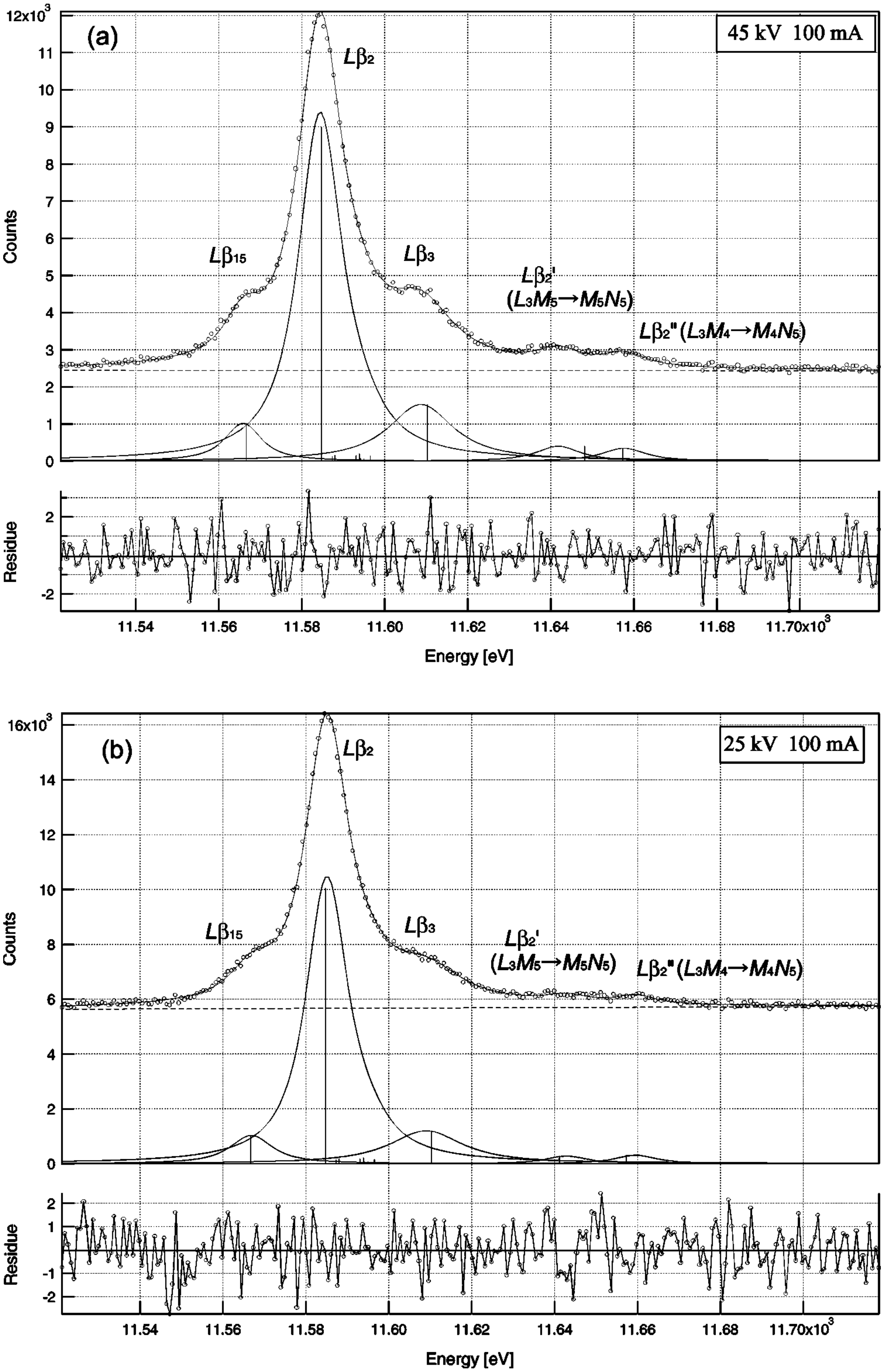

FIG. 1. Measured emission spectra of Au $L\beta_2$, $L\beta_3$, and $L\beta_{15}$ (a) excited at 45 kV and (b) excited at 25 kV.

(although this is strictly not correct, but is a crude estimation to describe quantitatively the simplest model of deexcitation).

The satellite lines are proposed to be caused by only a single Coster-Kronig transition. Multiple Coster-Kronig transitions, and a combination of the Coster-Kronig transition and the shake process can also occur within the ionization process. However, the combined processes can be ignored due to the low probabilities. When satellite lines are caused by a single Coster-Kronig transition, the intensity of the diagram line $L\beta_2$ can be calculated from

$$I_M(L\beta_2)=C\sigma_3\omega_3\frac{\Gamma(L\beta_2)}{\Gamma_3}, \quad (3)$$

where C is the constant, $\sigma_{i,i=1,2,3}$ are ionization cross sections by electrons of the L_i subshell, $\Gamma_{i,i=1,2,3}$ are total transition probabilities of the L_i subshell, and $\Gamma(L\beta_2)$ is the

TABLE II. Comparison of measured FWHM of Au L emission lines with other experimental and theoretical values. All units are in eV.

FWHM Line	Present work Single crystal	Double crystal	Williams (1934)[a]	Richtmyer (1934)[b]	Amorim (1988)[c]	Theoretical Value[d]
$L\alpha_1$	8.38 ± 0.02[e]	8.00 ± 0.02[e]	8.57	8.1	7.78 ± 0.12	7.72 ± 0.77
$L\alpha_2$	8.39 ± 0.09[e]	8.16 ± 0.09[e]		8.5	8.08 ± 0.16	7.72 ± 0.77
$L\beta_1$	8.67 ± 0.03	(7.9 ± 0.1)[f]	8.28	7.75	8.20 ± 0.21	7.71 ± 0.77
$L\beta_2$	11.4 ± 0.1[e]	(10.8 ± 0.1)[f]	11.4	10.3	10.12 ± 0.15	9.44 ± 1.54
$L\beta_3$	18.4 ± 0.7	(18.0 ± 0.1)[f]		20.8	16.48 ± 0.57	18.3 ± 4.1

[a]Reference [2].
[b]Reference [3].
[c]Reference [6].
[d]Reference [15].
[e]Multiplet fitting.
[f]Derived from single-crystal data.

L_3-N_5 transition probability. For $L\beta_2$ satellite lines, the transition to the initial vacancy state L_3 can occur by two possible Coster-Kronig transitions, L_1-L_3X and L_2-L_3X. The intensity of each spectator hole satellite line consists of the following two terms

$$I_S(L\beta_2)=C\sigma_1 f_{1,3}P(L_1L_3X)\,\omega_3\frac{\Gamma(L\beta_2)}{\Gamma_3}+C\sigma_2 f_{2,3}P(L_2L_3X)\,\omega_3\frac{\Gamma(L\beta_2)}{\Gamma_3}, \tag{4}$$

where $f_{i,j}$ is the partial Coster-Kronig transition probability from level L_i to level L_j and $P(L_iL_jX)$ is the probability of the radiationless transition L_i-L_jX that results in the double vacancy state L_jX. The intensity of each satellite line relative to the diagram line $L\beta_2$ can be expressed as

$$\frac{I_S}{I_M}=\frac{\sigma_1}{\sigma_3}f_{1,3}P(L_1L_3X)+\frac{\sigma_2}{\sigma_3}f_{2,3}P(L_2L_3X). \tag{5}$$

This equation is applicable to all transitions from the initial L_3-shell vacancy.

Considering the influence of the shake-off process, the intensity of $L\beta_2$ and each of the satellite lines can be expressed as

$$I_M(L\beta_2)=C\sigma_3(1-Q_3)\,\omega_3\frac{\Gamma(L\beta_2)}{\Gamma_3}, \tag{6}$$

$$I_S(L\beta_2)=C\{\sigma_3Q_3(X)+\sigma_1(1-Q_1)f_{1,3}P(L_1L_3X)+\sigma_2(1-Q_2)f_{2,3}P(L_2L_3X)\}\,\omega_3\frac{\Gamma(L\beta_2)}{\Gamma_3}, \tag{7}$$

where $Q_i(X)$ is the probability of shake-off from the X orbital when a hole is created in the L_i subshell, and Q_i is the sum of the shake-off probabilities from all possible orbitals when a hole is created in the L_i subshell. The intensity of each satellite line relative to the diagram line $L\beta_2$ can then be expressed as

$$\frac{I_S}{I_M}=\frac{1}{1-Q_3}\left\{Q_3(X)+\frac{\sigma_1}{\sigma_3}(1-Q_1)f_{1,3}P(L_1L_3X)+\frac{\sigma_2}{\sigma_3}(1-Q_2)f_{2,3}P(L_2L_3X)\right\}. \tag{8}$$

Values reported by Krause were used for ω_i [17]. For σ_i, values reported by Pálinkás and Schlenk [18] at 60 keV were used, and for $P(L_iL_jX)$ values reported by Chen *et al.* [19] for $_{80}$Hg were used. Values reported by Krause were again used for $f_{i,j}$ [17], with values related to the shake-off process taken from calculations by Parente *et al.* [20]. Table III shows values obtained from these equations.

Measured spectra are shown in Fig. 1. Two satellite lines were confirmed in the region of rather high energy around the $L\beta_2$ diagram line. The numbers of satellite lines in the spectra agree with calculation results. This suggests that both L_1-L_3M_5 and L_1-L_3M_4 Coster-Kronig transition channels are open in gold [7].

The dependence of relative intensity I_S to $L\beta_2$ on excitation energy is shown in Fig. 2, where I_S is the sum of the intensities of the visible satellites, and $L\beta_2$ line intensity includes hidden satellites. The I_S of $L\beta_2$ exhibits a gentle increase with excitation voltage and becomes constant above around 40 kV. The Coster-Kronig factor $f_{1,3}$ is constant in this energy region and the satellite intensity due to this process is independent of excitation energy. Shake-off process probabilities $Q_1(X)$, on the other hand, are positively correlated with excitation energy, but become almost independent

TABLE III. Theoretical average energies (eV) (from Ref. [16]) and relative intensities [from Eq. (8)] of Au $L\beta_2$ satellite lines due to a single *M*, *N*, *O*, or *P* shell spectator hole.

Spectator hole	Energy of $L\beta_2$ satellites [a] (eV)	Relative intensity (%)			
			Shake-off	Coster-Kronig	
X	L_3X-N_5X	Total	L_3X [b]	$L_1 \rightarrow L_3X$	$L_2 \rightarrow L_3X$
Nowhere[c]	11 584.7[d]	100	100	100	100
M_1	11 643.79	0.020	0.020	0	0
M_2	11 654.96	0.028	0.028	0	0
M_3	11 639.47	0.056	0.056	0	0
M_4	11 657.49	5.7	0.067	5.6	0
M_5	11 648.35	7.6	0.10	7.5	0
N_1	11 595.01	0.74	0.075	0.44	0.22
N_2	11 596.55	1.8	0.11	0.18	1.5
N_3	11 594.12	0.93	0.22	0.27	0.44
N_4	11 593.88	2.7	0.41	0.68	1.6
N_5	11 593.08	2.0	0.61	0.84	0.56
$\Sigma(N_1$-$N_5)$	11 594.37	8.2	1.4	2.4	4.4
N_6	11 587.35	1.8	1.1	0.54	0.10
N_7	11 588.02	2.2	1.5	0.67	0.043
$\Sigma(N_6$-$N_7)$	11 587.73	3.9	2.6	1.2	0.14
O_1		0.39	0.26	0.087	0.043
O_2		0.82	0.53	0.032	0.26
O_3		1.2	1.1	0.048	0.076
O_4		15	15	0.070	0.17
P_1		6.5	6.5	0.0093	<0.0001
$\Sigma(O_1$-$P_1)$		24	23	0.25	0.55

[a]Interpolation, from Ref. [16].
[b]Shake-off process, Ref. [20].
[c]Diagram line.
[d]Reference [12].

of excitation energy at high enough energies for multiple ionization.

The dependence on excitation energy of the intensity of $L\beta_3$ relative to $L\beta_2$ and the intensity of I_S relative to $L\beta_3$ are also shown in Fig. 2. Intensity of the $L\beta_3$ line relative to the $L\beta_2$ line exhibits a tendency similar to the intensity of I_S relative to $L\beta_2$. However, the intensity I_S relative to $L\beta_3$ seems to be almost constant, independent of excitation energy. This suggests that the increase in intensity I_S relative to $L\beta_2$ can be ascribed to the same origin as the intensity of $L\beta_3$ relative to $L\beta_2$. Considering that $P(L_2L_3M_X)$ is zero (see Table III), the intensities of $L\beta_3$ relative to $L\beta_2$ and I_S relative to $L\beta_3$ can be expressed in the same way as

$$\frac{I_M(L\beta_3)}{I_M(L\beta_2)}=\frac{\sigma_1}{\sigma_3}\,\frac{1-Q_1}{1-Q_3}\,\frac{\omega_1}{\omega_3}\,\frac{\Gamma_3\Gamma(L\beta_3)}{\Gamma_1\Gamma(L\beta_2)}, \tag{9}$$

$$\frac{I_S}{I_M(L\beta_3)}=\left\{\frac{\sigma_3}{\sigma_1}\,\frac{Q_3(M)}{1-Q_1}+f_{1,3}P(L_1L_3M)\right\}\frac{\omega_3}{\omega_1}\,\frac{\Gamma_1\Gamma(L\beta_2)}{\Gamma_3\Gamma(L\beta_3)}. \tag{10}$$

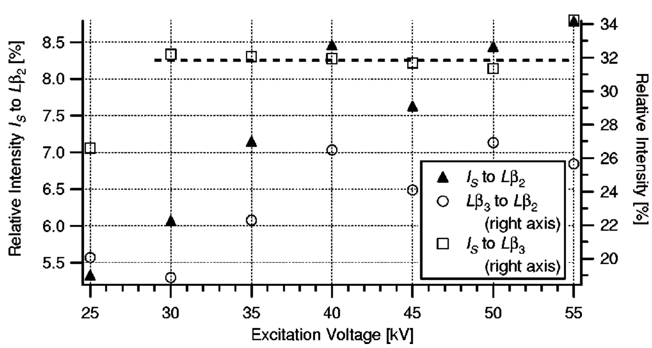

FIG. 2. Relative intensity as a function of excitation electron voltage for ▲ [I_S (sum of $L\beta_2$ visible satellites) to $L\beta_2$], ○ ($L\beta_3$ to $L\beta_2$), and □ (I_S to $L\beta_3$) points. The dashed line is a fit to the □ points.

From Eqs. (8) and (9), the tendency observed in Fig. 2 can be seen to originate from the common term $(\sigma_1/\sigma_3)[(1-Q_1)/(1-Q_3)]$. This experiment shows that the observed $I_S/[I_M(L\beta_3)]$ is almost constant in the region of 25 to 55 kV. This means that the contribution of the shake-off process is very small, because only the term $(\sigma_3/\sigma_1)[Q_3(M)/(1-Q_1)]$ depends on excitation energy in the right-hand side of Eq. (10). Therefore, the increase in the intensity I_S relative to $L\beta_2$ is not due to a shake-off process but due to the ratio of the ionization cross sections of subshells L_1 and L_3, and the ratio σ_1/σ_3 can be thought of as a constant for excitation

TABLE IV. Measured and theoretical energy values of visible satellite lines.

Satellite line	Spectator hole	Energy (eV) Measured	Energy (eV) Theory	Relative intensity (%) Measured	Relative intensity (%) Theory
$L\beta_2'$	M_5	11641.7 ± 1.1	11648.4	4.1 ± 0.4	5.5
$L\beta_2''$	M_4	11658.1 ± 1.2	11657.5	4.1 ± 0.8	4.2

voltages of over 40 kV. Satellite lines whose origins are dominantly ascribed to Coster-Kronig transitions are thought to exhibit similar dependencies on excitation energy.

Measured and theoretical energies and relative intensities of the visible satellite lines are given in Table IV. Theoretical values of the $L\beta_2''$ satellite line are in good agreement with observations. Effects of the shake-off process were also found to be small in the excitation energy region of 25 to 55 kV. However, the measured intensity of $L\beta_2'$ is smaller than the theoretical value. Tails of the $L\beta_2$ and $L\beta_3$ spectra possibly affect the fitted intensity of the $L\beta_2'$ satellite lines because $L\beta_2'$ exists near the two diagram lines. The calculated energy value of $L\beta_2''$ is also consistent with observations. However, calculated and measured energies of $L\beta_2'$ are considerably different. In particular, in $L\beta_2'$ the difference is bigger than that in $L\beta_2''$. Since M_5, the spectator hole of $L\beta_2'$, is nearer the outer shell than M_4, M_5 is more easily influenced by the atomic environment. Theoretical energies can be calculated for atomic states that do not have this influence.

IV. CONCLUSIONS

Visible $L\beta_2$ satellite lines in Au are mainly caused by L_1-L_3M_i ($i=4,5$) Coster-Kronig transitions, whereas the effect of the shake-off process is negligibly small. Comparison of the satellite lines with diagram lines from the L_1 subshell, such as $L\beta_3$ spectrum, is significant to the elucidation of the origins of the satellite lines.

Satellite lines that are mainly due to Coster-Kronig transition(s) can be thought of as exhibiting the same excitation energy dependence as the gold $L\beta_2$ satellite lines measured. This result could then be used as a standard for the origin of satellite lines of other elements.

A discrepancy between the theoretical and experimental values of the energy of the $L\beta_2'$ line was found. To probe this, discrepancy measurements of the $L\beta_2$ satellite lines of other heavy elements need to be conducted.

In electron bombardment, photon flux at the expected excitation energy is very small. Therefore, spectra excited at energies near the threshold cannot be measured using this system. In the near future, to elucidate the mechanisms behind the visible satellites of $L\beta_2$ for $_{79}$Au in detail, x-ray emission spectra will be studied as a function of incident photon energy using tunable synchrotron radiation sources. In particular, great interest lies in measuring spectra excited at a photon energy near the threshold of the $_{79}$Au $L\beta_2$ satellite lines. Such work is also expected to allow more accurate measurement of energies and relative intensities of satellite lines. Similar experiments also need to be performed for the near-Z elements $_{77}$Ir and $_{78}$Pt.

[1] T.D. Thomas, Phys. Rev. Lett. **52**, 417 (1987).
[2] J.H. William, Phys. Rev. **45**, 71 (1934).
[3] F.K. Richtmyer, S.W. Barnes, and E. Ramberg, Phys. Rev. **46**, 843 (1934).
[4] J.N. Cooper, Phys. Rev. **61**, 234 (1942).
[5] M.L. Carvalho, F. Parente, and L. Salgueiro, J. Phys. B **20**, 935 (1987).
[6] P. Amorim, L. Salgueiro, F. Parente, and J.G. Ferreira, J. Phys. B **21**, 3851 (1988).
[7] M.H. Chen *et al.*, At. Data Nucl. Data Tables **19**, 97 (1977).
[8] L. Salgueiro, M.L. Carvalho, and F. Parente, J. Phys. (Paris), Colloq. **48**, C9-609 (1987).
[9] A.M. Vlaicu *et al.*, Phys. Rev. A **58**, 3544 (1998).
[10] A.M. Vlaicu *et al.* (private communication).
[11] J.A. Bearden and A.F. Burr, Rev. Mod. Phys. **39**, 125 (1967).
[12] J.A. Bearden, Rev. Mod. Phys. **39**, 78 (1967).
[13] T. Tochio, Y. Ito, and K. Omote, Phys. Rev. A **65**, 042502 (2002).
[14] M. Deutsch, G. Hölzer, J. Härtwig, J. Wolf, M. Fritsch, and E. Förster, Phys. Rev. A **51**, 283 (1995).
[15] J.L. Campbell and T. Papp, At. Data Nucl. Data Tables **77**, 1 (2001).
[16] F. Parente, M.H. Chen, and B. Crasemann, At. Data Nucl. Data Tables **26**, 383 (1981).
[17] M.O. Krause, J. Phys. Chem. Ref. Data **8**, 307 (1979).
[18] J. Pálinkás and B. Schlenk, Z. Phys. A **297**, 29 (1980).
[19] M.H. Chen *et al.*, At. Data Nucl. Data Tables **24**, 13 (1979).
[20] F. Parente, M.L. Carvalho, and L. Salugueiro, J. Phys. B **16**, 4305 (1983).